

Accepted Manuscript

Effect of magnetic field on the hydrodynamic and heat transfer of magnetite ferrofluid flow in a porous fin heat sink

Mojtaba Bezaatpour, Mohammad Goharkhah

PII: S0304-8853(18)32080-8

DOI: <https://doi.org/10.1016/j.jmmm.2019.01.028>

Reference: MAGMA 64831

To appear in: *Journal of Magnetism and Magnetic Materials*

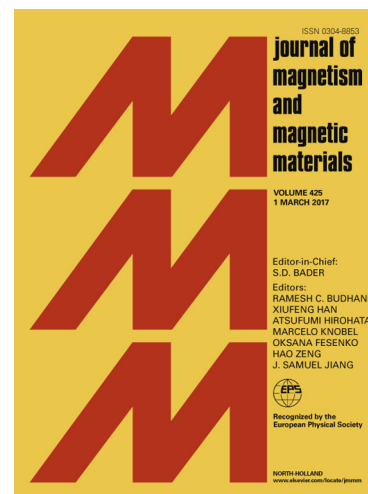
Received Date: 30 June 2018

Revised Date: 29 October 2018

Accepted Date: 7 January 2019

Please cite this article as: M. Bezaatpour, M. Goharkhah, Effect of magnetic field on the hydrodynamic and heat transfer of magnetite ferrofluid flow in a porous fin heat sink, *Journal of Magnetism and Magnetic Materials* (2019), doi: <https://doi.org/10.1016/j.jmmm.2019.01.028>

This is a PDF file of an unedited manuscript that has been accepted for publication. As a service to our customers we are providing this early version of the manuscript. The manuscript will undergo copyediting, typesetting, and review of the resulting proof before it is published in its final form. Please note that during the production process errors may be discovered which could affect the content, and all legal disclaimers that apply to the journal pertain.



Effect of magnetic field on the hydrodynamic and heat transfer of magnetite ferrofluid flow in a porous fin heat sink

Mojtaba Bezaatpour^a, Mohammad Goharkhah^{a,*}

^a **Department of Mechanical Engineering, Sahand University of Technology, Tabriz, Iran**

ACCEPTED MANUSCRIPT

*Corresponding Author at: Department of Mechanical Engineering, Sahand University of Technology, Tabriz, Iran, Tel. : +98 4133458449, Email: goharkhah@sut.ac.ir.

Effect of magnetic field on the hydrodynamic and heat transfer of magnetite ferrofluid flow in a porous fin heat sink

Abstract

The present study numerically investigates the effects of a uniform external magnetic field and porous fins on convective heat transfer and pressure drop of magnetite (Fe_3O_4 /water) nanofluid in a heat sink. Effects of volume fraction, porosity, Reynolds number, and magnetic field strength on the performance of the heat sink are studied. Results indicate that heat transfer increases at high volume fractions, fin porosities and magnetic field intensities and decreases with the Reynolds number. A 13% enhancement of heat transfer is obtained for the heat sink with solid fins by using ferrofluid compared to the pure water flow. This value grows up to 35% by using porous fins and imposing magnetic field to the heat sink. Moreover, using porous fins is shown to decrease the pressure drop while the magnetic field effect is not considerable. Therefore, it is concluded that the proposed methods result in a remarkable heat transfer enhancement while decreasing the pressure drop.

Key words: Heat sink, porous fins, magnetic field, heat transfer, magnetite ferrofluid

1. Introduction

Ferrofluid is a colloidal mixture of magnetic nanoparticles in a carrier liquid typically water or oil that becomes strongly magnetized in the presence of an external magnetic field. Ferrofluid has been used in several applications such as loud speakers, accelerometers, flow meters, rotary seals, and pumps [1]. However, a remarkable attention has been paid in the recent past on the employment of ferrofluid as a coolant in thermal management of electronics and heat exchangers for two reasons. Firstly, an external magnetic field can improve the thermal conductivity of ferrofluid [2]. Secondly, ferrofluid flow and consequently heat transfer can be controlled and enhanced by an appropriate magnetic field source [3]. Possibility of free convection heat transfer enhancement using ferrofluids has been investigated considering different geometries such as cubic enclosure [4], rectangular cell with different aspect ratios [5,6], cylindrical [7], annular [8], and triangular [9] enclosures. Li and Xuan [10] experimentally studied the effect of both uniform and non-uniform magnetic fields on convective heat transfer of Fe_3O_4 /water nanofluid around a heated fine wire. Their result showed an increased heat exchange between the ferrofluid and heated wire by applying a non-uniform magnetic field while the heat transfer was weakened in the presence of a uniform magnetic field. Experimental and numerical investigations were performed by Zablockis et al. [11] on thermomagnetic convection in a heated cylinder under the magnetic

field of a solenoid. They observed heat transfer enhancement up to seven fold under the magnetic field. Jafari et al. [12] investigated the effect of different parameters on the thermomagnetic convection in a cylindrical geometry using the Taguchi technique. They performed a verification test to confirm the validity of the used statistical method and obtained the optimum conditions for heat transfer enhancement.

Forced convection heat transfer in the presence of an external magnetic field has also been the subject of few researches. Effect of an external magnetic field on the convective heat transfer of Fe_3O_4 /water ferrofluid flowing through a tube was investigated by Lajvardi et al. [13]. Their experimental results indicated the influence of ferrofluid concentration and magnet position on the Nusselt number. Azizian et al. [14] studied on the effect of a constant magnetic field on the laminar convective heat transfer and pressure drop of magnetite nanofluid in a vertical tube and reported a considerable heat transfer enhancement of 300% against only a 7.5% increase of pressure drop. They also showed that the convective heat transfer enhancement increases with the magnetic field intensity and gradient. Ferrofluid flow in a miniature circular heat sink under the influence of uniform magnetic field was studied experimentally by Ashjaee et al. [15]. Their results indicated 14% and 38% heat transfer improvement compared to the pure water, in the absence and presence of magnetic field, respectively. Xuan et al. [16] calculated the flow and temperature distribution of a ferrofluid in a microchannel under the influence of magnetic field gradient using lattice-Boltzmann method. It was shown that heat transfer augmentation depends on the magnitude and direction of the magnetic force. Ganguly et al. [17] and Strek and Jopek [18] carried out two dimensional numerical studies and simulated the constant external magnetic field by a line-source dipole. They showed that the non-uniform magnetic body force resulted from spatial variation of the magnetization causes the formation of local vortices. The vortices were shown to alter the advection energy transport and increase the heat transfer. Effect of an alternating magnetic field on the forced convection heat transfer of water based Fe_3O_4 ferrofluid was investigated by Ghofrani et al. [19] and Goharkhah and Ashjaee [20]. They obtained the heat transfer enhancement as a function of magnetic field strength, frequency and Reynolds numbers and reported 27.6% and 13.9% heat transfer enhancement, respectively. Bahiraei and Hangi [21] numerically studied the hydrothermal characteristics of a ferrofluid in a toroidal loop consists of two heat sources and heat sinks in the presence of magnetic field. Different parameters including heat flux, temperature of heat sink, magnet position and strength were studied.

Review of the previous works reveals that application of magnetic field for natural and forced convection heat transfer enhancement has been studied only in simple and classical geometries. The geometry of the current study is a 3D heat sink which has many applications in the electronics cooling. The solid fins of

the hit sink are also replaced by porous fins in order to decrease the pressure drop while increasing the heat transfer. Moreover, the magnetic field is assumed to be generated by an electromagnet. This magnetic field source is not encountered in the previous works. Separate and combined effects of these active and passive heat transfer methods are investigated at different Reynolds numbers, volume fractions and magnetic field intensities.

2. Problem description

An aluminum heat sink with length, width, and height of 40, 40 and 10 mm respectively, is used in the numerical simulations, as shown in Fig. 1(a). The heat sink consists of five channels and aluminum porous fins with rectangular cross section. The detailed dimensions are summarized in Table 1. A uniform heat flux of 66 kW/m² is imposed from the bottom surface while the other surfaces are insulated. The heat sink is assumed to be placed in the air gap of a U shape electromagnet as shown in Fig. 1 (a). A uniform magnetic field in Y direction is generated in the center of the air gap and far from the electromagnet tips. The magnetic field at different intensities is applied to the ferrofluid flowing through the heat sink in Z direction. More details on the electromagnet can be found in ref. [15]. The physical properties of porous material and magnetite nanoparticle have been summarized in Table 2.

3. Governing equations and boundary conditions

3.1. Governing equations

The steady state and homogeneous form of the continuity, momentum, and energy equations for the fluid and porous domains can be written as follows.

$$\nabla \cdot (\rho_f V) = 0 \quad (1)$$

$$\frac{\rho_f}{\varepsilon} \frac{(V \cdot \nabla)V}{\varepsilon} = -\nabla P + \frac{\mu}{\varepsilon} \nabla^2 V - \frac{\mu}{K_p} V - \frac{C_f \rho_f}{K_p^{1/2}} |V|V + (M \cdot \nabla)B \quad (2)$$

$$(\rho C_p)_{eff} V \cdot \nabla T = \nabla \cdot (k_{eff} \nabla T) \quad (3)$$

The effective specific heat and conductivity of the porous domain are calculated from:

$$(\rho C_p)_{eff} = (1 - \varepsilon)(\rho C_p)_s + \varepsilon(\rho C_p)_f \quad (4)$$

$$k_{eff} = (1 - \varepsilon)k_s + \varepsilon k_f \quad (5)$$

It is assumed that the solid and the fluid phases are at thermal equilibrium. The energy equation for the solid domain is written as:

$$k_s \left(\frac{\partial^2 T_s}{\partial x^2} + \frac{\partial^2 T_s}{\partial y^2} + \frac{\partial^2 T_s}{\partial z^2} \right) = 0 \quad (6)$$

The third and fourth terms on the right hand side of Eq. 2 are Darcy and Forchheimer terms for porous media, respectively [22]. Moreover, the last term in this equation is the magnetic volume force or so called Kelvin body force that is calculated as follows.

3.2. Magnetic body force

Maxwell's equations for a non-conducting fluid can be written as:

$$\nabla \cdot B = 0 \quad (7)$$

$$\nabla \times H = 0 \quad (8)$$

The relation between B, H and M is stated as:

$$B = \mu_0(M + H) \quad (9)$$

It is often possible to assume that the magnetization vector is aligned with the magnetic field. Thus:

$$M = \chi_m H \quad (10)$$

where, χ_m is the magnetic susceptibility and is obtained from [17]:

$$\chi_m(T) = \frac{\chi_0}{1 + \beta(T - T_0)} \quad (11)$$

By using equations (9), (10), and (11) the magnetic body force in the momentum equation can be written as:

$$F_k = \frac{1}{2} \mu_0 \chi_m (1 + \chi_m) \nabla(H \cdot H) + \mu_0 \chi_m H ((H \cdot \nabla) \chi_m) \quad (12)$$

The magnetic field at the center of the electromagnet air gap where the heat sink is located has only a uniform component in Y direction [15]. Thus, the magnetic body force can be simplified as follows.

$$F_k = \mu_0 \chi_m H^2 \frac{-\chi_0 \beta}{[1 + \beta(T - T_0)]^2} \frac{\partial T}{\partial y} \hat{j} \quad (13)$$

Eq. 13 indicates that the resulting magnetic force has a single component in Y direction due to the temperature dependent magnetic susceptibility.

3.3. Boundary conditions

The ferrofluid with constant inlet temperature of 298K and uniform velocity flows into the heat sink through the channels and is subjected to the uniform heat flux of 66 kW/m² from bottom surface of the heat sink. The nanofluid is at the atmospheric pressure at the channel outlet. The no-slip condition exists at all fluid solid interfaces:

$$V = 0, T_f = T_s, \quad -k_{eff} \frac{\partial T_f}{\partial n} = -k_s \frac{\partial T_s}{\partial n} \quad (14)$$

Moreover, the condition at the insulated walls is expressed as:

$$\frac{\partial T}{\partial n} = 0 \quad (15)$$

4. Thermophysical properties

The nanofluid properties such as density, specific heat, viscosity are calculated as a function of temperature and nanoparticle volume fraction from the following equations [23].

$$\rho_{nf} = (1 - \varphi)\rho_f + \varphi\rho_{np} \quad (16)$$

$$(\rho C_p)_{nf} = (1 - \varphi)(\rho C_p)_f + \varphi(\rho C_p)_{np} \quad (17)$$

$$\mu_{nf} = \mu_f(1 + 2.5\varphi) \varphi \leq 2\% \quad (18a)$$

$$\mu_{nf} = \frac{\mu_f}{(1 - \varphi)^{2.5}} \varphi > 2\% \quad (18b)$$

where, the indices f, np, and nf refer to the base fluid, nanoparticle and nanofluid, respectively. Also, the thermal conductivity is calculated from [24]:

$$k_{nf} = k_{Static} + k_{Brownian} \quad (19a)$$

$$k_{Static} = k_f \left[\frac{(k_{np} + 2k_f) - 2\varphi(k_f - k_{np})}{(k_{np} + 2k_f) + \varphi(k_f - k_{np})} \right] \quad (19b)$$

$$k_{Brownian} = 5 \times 10^4 \beta \varphi \rho_f C_{p,f} \sqrt{\frac{kT}{\rho_{np} D_{np}}} g(\varphi, T) \quad (19c)$$

where, $k = 1.3807 \times 10^{-23}$ J/K and β is the fraction of the liquid volume which travels with a particle, while:

$$g = (-6.04\varphi + 0.4705)T + 1722.3\varphi - 134.63 \quad (19d)$$

Worth mentioning that, thermophysical properties of pure water in the above equations have been assumed to be temperature dependent. Finally, the local heat transfer coefficient is calculated from the following equation.

$$h = \frac{q''}{\Delta T} = \frac{q''}{T_w - T_m} \quad (20)$$

Where, q'' is the surface heat flux and T_w and T_m are the surface and bulk flow temperatures, respectively.

5. Numerical modeling, grid independency and validation of the numerical method

The set of three dimensional governing equations with the prescribed boundary conditions are solved using finite volume method. A structured non-uniform grid is used in the simulations, as shown in Fig. 1(b). The grid points are clustered near the channel walls where the velocity and temperature gradients are large. The solver specifications for discretization of the domain involve the SIMPLE algorithm for pressure- velocity coupling and second-order upwind for both momentum and energy equations. Moreover, the residual levels are lowered to $10e^{-6}$ for the velocities and energy equation to ensure the accuracy.

In order to check the grid independency, the primary simulations are carried out using different grid numbers of 272340, 500440, and 1123560 for discretization of the computational domain. Fig. 2(a) shows the velocity distribution in the porous fins and the channels for different grid sizes at $Re = 1040$, $\phi = 2\%$, and $\varepsilon = 0.95$. Furthermore, the bottom surface temperature along the channels in the z direction is presented in Fig. 2 (b) for different grid numbers.

Fig. 2(a) and (b) indicate that the difference between the results obtained from several grid numbers is negligible. Thus, the grid distribution with 500440 grids has been used in the simulations. Also worth mentioning in Fig. 2(a) is the nonzero velocity at the fin- channel interface due to the flow penetration into the porous fins.

Two different experimental cases are considered for validating the current numerical results. These cases are the experimental results of Jiang et al. [25] for a parallel plate porous channel with porosity of $\varepsilon=0.44$ and that of Ashjaee et al. [15] for a miniature heat sink with magnetite ferrofluid as a coolant under the magnetic field effect. It should also be noted that the geometry, dimensions, boundary conditions, working fluid, and the external magnetic field of the current study is selected based on the ref. [15]. Therefore, it is the most relevant experimental case for validation. Comparison between the numerical results and the experimental data of refs. [25] and [15] is shown in Figs. 3 and 4, respectively.

Fig. 3(a) shows the pressure drop variation in the porous channel with Reynolds number. The local Nusselt number variation on the porous channel surface is also shown in Fig. 3(b) for two different Reynolds numbers.

Fig. 4(a) shows the pressure drop variation along the heat sink length for different Reynolds numbers at $\varphi = 2\%$ and $B = 800\text{G}$. The local heat transfer coefficient in the absence and presence of the external magnetic field for $\text{Re} = 600$ and $\varphi = 3\%$ is also illustrated in Fig. 4(b).

The maximum deviation from the experimental results has been found to be less than 8%. The agreement between the numerical and experimental results, as seen in Figs. 3 and 4 indicates that the ferrofluid flow, porous media, and the external magnetic field effects on the pressure drop and heat transfer can be predicted by the current numerical method with a reasonable accuracy.

6. Results and discussion

Numerical simulations are carried out for different fin porosities of $\varepsilon = 0.75, 0.80, 0.85, 0.90,$ and 0.95 , ferrofluid volume fractions of $\varphi = 1, 2,$ and $3\text{Vol}\%$ and Reynolds numbers between 200 and 1200. The magnetic field intensity is varied in the range of $B = 0 - 1600\text{ G}$.

6.1. Magnetic force distribution

The magnetic field is uniform in the center of the electromagnet air gap where the heat sink is assumed to be located. Thus, the resulting magnetic force will have a single component in the vertical direction, Y due to the temperature dependent magnetic susceptibility of the ferrofluid as mentioned in Eq. 11. More details on the magnetic field simulation can be found in ref. [15]. Magnetic force variation in the flow direction, Z is depicted for two cases of solid fin and porous fin heat sinks with $\varepsilon = 0.90$ in Fig. 5(a). Moreover, Fig. 5(b) shows the magnetic body force variation in the Y direction at the channels outlet.

Since the magnetic force is a function of temperature gradient, different curves are obtained for the cases of solid and porous fins, as shown in Fig. 5 (a) and (b). Fig. 5(a) indicates that the magnetic force is very intense at the channel inlet due to the high temperature gradient between the bottom surface and the cold fluid entering the channel. However, it decays gradually as the boundary layer grows and the fluid temperature rises. Similarly, higher temperature gradients at the vicinity of bottom surface than that of the insulated top surface has resulted in a higher magnetic force at the bottom half of the channels as shown in Fig. 5(b).

6.2. Heat transfer and hydrodynamic results

In order to visualize the effect of above mentioned magnetic force distribution on the flow field, velocity contours and vectors in the symmetry plane of the heat sink are depicted for $B = 0\text{G}$ and $B = 1600\text{G}$ cases in Fig. 6.

Comparison of Figs. 6(a) and (b) illustrates that the higher magnetic force near the bottom surface as mentioned in Fig. 5, has disturbed the velocity field in this region while a little change is observed below the top surface. It is also observed that the magnetic field has not a considerable influence on the flow field near the channel inlet where the boundary layer is thin and the velocity is almost uniform. On the other hand, with development of hydrodynamic boundary layer and growth of the low velocity region the effect of magnetic field becomes more pronounced. The total effect of the positive magnetic force is to remove the hot fluid from the neighborhood of the hot wall while bring the cool fluid from the bulk flow. This phenomenon is the main mechanism of heat transfer enhancement in the presence of the external magnetic field.

In order to better explain the effect of the magnetic field on the ferrofluid, the velocity contours at the middle channel outlet under different magnetic field intensities are shown in Fig. 7.

It can be inferred from Fig. 7 that the magnetic field decreases the size of high velocity region, moves it away from the bottom surface and increases the maximum velocity as a result.

Variation of the velocity profile at the outlet of the middle channel with magnetic field intensity is plotted for solid and porous fin heat sinks in Fig. 8(a) and (b), respectively.

Fig. 8 shows that an asymmetric velocity profile results due to the external magnetic field. It is also shown that the ferrofluid velocity near the heated surface decreases with increase of the magnetic field intensity. This allows the ferrofluid to absorb the heat from the bottom surface more efficiently.

Due to the change of flow field under the external magnetic field, the temperature distribution and heat transfer characteristics are also expected to be influenced. Effect of the magnetic field on the temperature distribution in the middle channel is shown in Fig. 9(a) and (b).

Fig. 9 indicates that the vertical magnetic field removes the hot fluid from the bottom surface. This disturbs the thermal boundary layer and facilitates the heat advection to the bulk fluid.

Temperature distribution in the outlet of the middle channel under the influence of the magnetic field is shown in Fig.10 for $Re = 260$.

As shown in Fig. 10, the magnetic field tends to remove the hot fluid from the bottom surface and disrupts the thermal boundary layer. This allows the colder bulk fluid to replace the hot fluid and consequently improves the heat transfer.

Variation of the temperature along the bottom surface in the flow direction at $x = 0.02\text{m}$ is depicted in Fig. 11 for the cases of figure 10.

As shown in Fig. 11, the surface temperature is decreased with increase of the magnetic field intensity which means that the heat transfer is improved in the presence of magnetic field.

The average heat transfer coefficient is calculated for all the simulated cases by integrating the local heat transfer coefficient over the heat transfer area. Variations of the average heat transfer coefficient with Reynolds number and magnetic field strength for the solid and porous fin heat sinks are demonstrated in Fig. 12(a) and (b), respectively.

A similar trend can be observed in both figures. The average heat transfer coefficient increases in the presence of the magnetic field and has a direct relation with magnetic field strength. However, with increase of the Reynolds number, the ferrofluid flows with a higher velocity and the time it is influenced by the magnetic field is decreased. Therefore, the magnetic field is shown to have a greater effect on the heat transfer at low Reynolds numbers.

Effect of magnetic field on the convective heat transfer coefficient at different fin porosities and ferrofluid volume fractions is shown in Fig. 13.

Fig. 13 illustrates that the convective heat transfer changes slightly for porosities lower than 0.8 while it increases sharply for higher porosities. This can be justified considering the two main factors on the convective heat transfer, the contact area between the fluid and fin surface and the flow penetration into the porous fins. Increase of the fin porosity despite decreasing the heat transfer area, allows more fluid to penetrate into the fins. These effects counterbalance each other at low porosities. However, Fig. 13 implies that the flow penetration effect is more important at higher porosities and the convective heat transfer increases, consequently.

Variation of the pressure drop in the heat sink with Reynolds number, porosity, and volume fraction under the influence of magnetic field is depicted in Fig. 14.

Fig. 14 indicates that using porous fins decreases the pressure drop in the heat sink compared to the solid fin case. As mentioned in Fig. 2 the fluid velocity is nonzero at the surface of the porous fins. This virtual slip velocity reduces the wall friction and results in the decrease of the pressure drop.

It can also be observed that the magnetic field has a negligible effect on the pressure drop. Pressure drop increase in the presence of an external magnetic field is mainly due to the increase of viscosity [26]. Moreover, creation of the vortices that act like barriers in the flow field can also contribute as the second reason for the pressure drop increase. This is the case when the magnetic field is generated by a magnetic dipole source [17]. However, the current results have been obtained assuming that viscosity is only a function of temperature and concentration. Furthermore, the upward magnetic force tends to remove the

heated ferrofluid from the surface without creation of any vortex. Thus, the magnetic field has not resulted in considerable change of the pressure drop.

6.3. Heat transfer enhancement

Effect of using nanofluid, porous fins and magnetic field on the heat transfer can be determined by comparing the average heat transfer coefficient results with that of the pure water flowing into the solid fin heat sink in the absence of magnetic field. The heat transfer efficiency is defined as:

$$\eta = h/h_b \quad (21)$$

where, the index b refers to the condition of water flow in the solid fin heat sink in the absence of magnetic field. Effect of Reynolds number and magnetic field intensity on the heat transfer efficiency for the solid and porous fin heat sinks are shown in Figs. 15(a) and (b), respectively.

It is clear that for both solid and porous fin heat sinks, the heat transfer efficiency increases in the presence of magnetic field. However, the magnetic field effect is more significant at low Reynolds numbers. It can also be observed that the Reynolds number has opposite effects in solid and porous fin heat sinks. In the latter case, increase of Reynolds number causes ferrofluid penetration into the porous fins and consequently more efficient heat removal. On the other hand, it decreases the time that ferrofluid is influenced by the magnetic field. It can be inferred that the first factor is more important in porous fins. But, the effect of magnetic field influence time on the efficiency increases with the magnetic field intensity. That is, by increasing the magnetic field intensity, a high heat transfer enhancement with porous fins can be achieved even at low Reynolds numbers.

Fig. 16 indicates the effect of magnetic field on the heat transfer efficiency at different porosities and volume fractions for $Re = 260$.

Fig. 16 shows that the heat transfer efficiency increases with increasing the porosity and volume fraction. Therefore, the maximum heat transfer efficiency occurs at $\varepsilon = 0.95$ in the presence of the magnetic field. Results show a maximum 22% heat transfer enhancement for the solid fin heat sink at $Re = 260$ and $\phi = 3\%$, and $B = 1600G$ due to the combined effects of using ferrofluid and applying magnetic field. The heat transfer efficiency is shown to be increased up to 35% by using a porous fin heat sink at the same conditions.

Conclusion

Effects of an external magnetic field and porous fins on the hydrodynamic and heat transfer characteristics of magnetite ferrofluid flowing in a heat sink are investigated numerically. The following results are obtained.

- The magnetic field removes the hot fluid from the neighborhood of the heated surface and brings the cold fluid from the bulk flow, disrupts the thermal boundary layer and consequently improves the heat transfer.
- The magnetic field is shown to have a greater effect on the heat transfer at low Reynolds numbers.
- The convective heat transfer changes slightly at low porosities while it increases sharply at high porosities.
- Using porous fins decreases the pressure drop in the heat sink compared to the solid fin case.
- The magnetic field has a negligible effect on the pressure drop.
- A maximum 22% heat transfer enhancement is obtained for the solid fin heat sink at $Re = 260$, $\phi = 3\%$, and $B = 1600G$ due to the combined effects of using ferrofluid and applying magnetic field. The heat transfer efficiency is shown to be increased up to 35% by using a porous fin heat sink at the same conditions.
- In contrast to the conventional heat transfer techniques, the proposed methods results in considerable heat transfer enhancement while decreasing the pressure drop.

Nomenclature

B	magnetic flux density($N \cdot A^{-1} \cdot m^{-1}$)	η	heat transfer effectiveness
C_f	quadratic drag factor	χ_m	magnetic susceptibility
C_p	specific heat ($kJ \cdot kg^{-1} \cdot K^{-1}$)	χ_0	reference magnetic susceptibility
D	diameter (m)	ρ	density (kg/m^3)
F_K	Kelvin body force (N/m^3)	μ	dynamic viscosity ($N \cdot s/m^2$)
h	local heat transfer coefficient ($W/m^2 \cdot K$), heat sink high (m)	μ_0	permeability of free space (N/A^2)
H	magnetic field intensity ($A \cdot m^{-1}$)	ε	porosity
k	thermal conductivity ($W \cdot m^{-1} \cdot K^{-1}$)	β	liquid volume fraction (k^{-1})
K_p	permeability of porous media (m^2)		
M	magnetization($A \cdot m^{-1}$)	subscripts	
n	normal direction	b	solid fins with water fluid
P	pressure (Pa)		and no magnetic field effect
q''	heat flux applied to bottom surface of heat sink (W/m^2)	eff	effective
Re	Reynolds number	f	fluid
T	temperature (K)	m	bulk
V	velocity ($m \cdot s^{-1}$)	nf	nanofluid
x,y,z	directions	np	nanoparticle
Greek		s	solid
φ	volume fraction	w	bottom surface
		0	at reference(300K)

References

- [1] R.L. Bailey, FerroX Ltd., 11 West Way, Botley, Oxford OX2 0JB, United Kingdom, *J. Magn. Magn. Mater.* 39 (1983) 178–182.
- [2] A. Karimi, M. Goharkhah, M. Ashjaee, M.B. Shafii, Thermal Conductivity of Fe₂O₃ and Fe₃O₄ Magnetic Nanofluids Under the Influence of Magnetic Field, *Int. J. Thermophys.* 36 (2015) 2720–2739.
- [3] M. Bahiraei, M. Hangi, Investigating the efficacy of magnetic nanofluid as a coolant in double-pipe heat exchanger in the presence of magnetic field, *Energy Convers. Manag.* 76 (2013) 1125–1133.
- [4] S.M. Snyder, T. Cader, B.A. Finlayson, Finite element model of magnetoconvection of a ferrofluid, *J. Magn. Magn. Mater.* 262 (2003) 269–279.
- [5] H. Yamaguchi, Z. Zhang, S. Shuchi, K. Shimada, Heat transfer characteristics of magnetic fluid in a partitioned rectangular box, *J. Magn. Magn. Mater.* 252 (2002) 203–205.
- [6] H. Yamaguchi, I. Kobori, Y. Uehata, K. Shimada, Natural convection of magnetic fluid in a rectangular box, *J. Magn. Magn. Mater.* 201 (1999) 264–367.
- [7] E. Blums, A. Mezulis, G. Kronkalns, Magnetoconvective heat transfer from a cylinder under the influence of a nonuniform magnetic field, *J. Phys. Condens. Matter.* 20 (2008).
- [8] T. Sawada, H. Kikura, A. Saito, T. Tanahashi, Natural convection of a magnetic fluid in concentric horizontal annuli under nonuniform magnetic fields, *Exp. Therm. Fluid Sci.* 7 (1993) 212–220.
- [9] T. Tynjälä, A. Hajiloo, W. Polashenski, P. Zamankhan, Magnetodissipation in ferrofluids, *J. Magn. Magn. Mater.* 252 (2002) 123–125.
- [10] Q. Li, Y. Xuan, Experimental investigation on heat transfer characteristics of magnetic fluid flow around a fine wire under the influence of an external magnetic field, *Exp. Therm. Fluid Sci.* 33 (2009) 591–596.
- [11] D. Zablockis, V. Frishfelds, E. Blums, Numerical investigation of thermomagnetic convection in a heated cylinder under the magnetic field of a solenoid, *J. Phys. Condens. Matter.* 20 (2008).
- [12] A. Jafari, T. Tynjälä, S.M. Mousavi, P. Sarkomaa, CFD simulation and evaluation of controllable parameters effect on thermomagnetic convection in ferrofluids using Taguchi technique, *Comput. Fluids.* 37 (2008) 1344–1353.
- [13] M. Lajvardi, J. Moghimi-Rad, I. Hadi, A. Gavili, T. Dallali Isfahani, F. Zabihi, J. Sabbaghzadeh, Experimental investigation for enhanced ferrofluid heat transfer under magnetic field effect, *J.*

- Magn. Magn. Mater. 322 (2010) 3508–3513.
- [14] R. Azizian, E. Doroodchi, T. McKrell, J. Buongiorno, L.W. Hu, B. Moghtaderi, Effect of magnetic field on laminar convective heat transfer of magnetite nanofluids, *Int. J. Heat Mass Transf.* 68 (2014) 94–109.
- [15] M. Ashjaee, M. Goharkhah, L.A. Khadem, R. Ahmadi, Effect of magnetic field on the forced convection heat transfer and pressure drop of a magnetic nanofluid in a miniature heat sink, *Heat Mass Transf.* 51 (2015) 953–964.
- [16] Y. Xuan, Q. Li, M. Ye, Investigations of convective heat transfer in ferrofluid microflows using lattice-Boltzmann approach, *Int. J. Therm. Sci.* 46 (2007) 105–111.
- [17] R. Ganguly, S. Sen, I.K. Puri, Heat transfer augmentation using a magnetic fluid under the influence of a line dipole, *J. Magn. Magn. Mater.* 271 (2004) 63–73.
- [18] T. Streck, H. Jopek, Computer simulation of heat transfer through a ferrofluid, *Phys. Status Solidi.* 244 (2007) 1027–1037.
- [19] A. Ghofrani, M.H. Dibaei, A. Hakim Sima, M.B. Shafii, Experimental investigation on laminar forced convection heat transfer of ferrofluids under an alternating magnetic field, *Exp. Therm. Fluid Sci.* 49 (2013) 193–200.
- [20] M. Goharkhah, M. Ashjaee, Effect of an alternating nonuniform magnetic field on ferrofluid flow and heat transfer in a channel, *J. Magn. Magn. Mater.* 362 (2014) 80–89.
- [21] M. Bahiraei, M. Hangi, Automatic cooling by means of thermomagnetic phenomenon of magnetic nanofluid in a toroidal loop, *Appl. Therm. Eng.* 107 (2016) 700–708.
- [22] D. a. Nield, A. Bejan, *Convection in Porous Media*, 2013.
- [23] Y. Xuan, W. Roetzel, Conceptions for heat transfer correlation of nanofluids, *Int. J. Heat Mass Transf.* 43 (2000) 3701–3707.
- [24] J. Koo, C. Kleinstreuer, A new thermal conductivity model for nanofluids, *J. Nanoparticle Res.* 6 (2004) 577–588.
- [25] P.X. Jiang, M. Li, T.J. Lu, L. Yu, Z.P. Ren, Experimental research on convection heat transfer in sintered porous plate channels, *Int. J. Heat Mass Transf.* 47 (2004) 2085–2096.
- [26] L. Wang, Y. Wang, X. Yan, X. Wang, B. Feng, Investigation on viscosity of Fe₃O₄nanofluid under magnetic field, *Int. Commun. Heat Mass Transf.* 72 (2016) 23–28.

List of figures

Fig. 1. (a) Schematic of the heat sink, (b) grid distribution in the channels and porous fins.

Fig. 2. (a) Velocity distribution in the plane normal to the flow direction at $z = 0.02\text{m}$ (b) bottom surface temperature along the channels in the z direction obtained from different grid sizes.

Fig. 3. Experimental and numerical results of (a) pressure drop at different Reynolds number, (b) local Nusselt number obtained for a porous parallel plat channel with $\epsilon=0.44$ and water as a coolant.

Fig. 4. Experimental and numerical results of (a) pressure drop for different Reynolds number at $\phi = 2\%$ and $B = 800\text{G}$, (b) local convective heat transfer coefficient at $\phi = 3\%$ and $\text{Re} = 600$ with $B = 0$ and $B = 1200\text{G}$ for a miniature heat sink.

Fig. 5. Magnetic force variation at $\text{Re} = 260$, $B = 1200\text{G}$, and $\phi = 2\%$ (a) on the bottom surface of the channels, along the flow direction (b) at the channels outlet, in Y direction.

Fig. 6. Velocity contours and vectors in the symmetry plane of the middle channel along the flow direction at $\phi = 2\%$ and $\text{Re} = 260$ in the absence and presence of magnetic field.

Fig. 7. Velocity contour at the middle channel outlet of the solid fin heat sink for $\phi = 2\%$ and $\text{Re} = 260$.

Fig. 8. Effect of magnetic field intensity on the velocity profile at the outlet of the middle channel for (a) solid and (b) porous fin heat sink with $\epsilon = 0.90$ at $\text{Re} = 260$, and $\phi = 2\%$.

Fig. 9. Ferrofluid temperature distribution along the flow direction in the symmetry plane of the middle channel for $\phi = 2\%$ and $\text{Re} = 260$ in the absence and presence of magnetic field.

Fig. 10. Effect of the magnetic field on the temperature distribution at the middle channel outlet of the solid fin heat sink for $\phi = 2\%$ and $\text{Re} = 260$.

Fig. 11. Surface temperature variation in the flow direction at $x = 0.02\text{m}$ at different magnetic field intensities.

Fig.12. Average heat transfer coefficient variation with Reynolds number and magnetic field strength at $\phi = 2\%$ for (a) non-porous heat sink, (b) porous heat sink with $\epsilon = 0.90$.

Fig. 13. Magnetic field effect on the average heat transfer coefficient at different porosities and volume fractions for $\text{Re} = 260$.

Fig. 14. Pressure drop as a function of (a) Reynolds number and magnetic flux density at $\phi = 2\%$, (b) porosity and volume fraction in magnetic field of $B = 1200\text{G}$.

Fig. 15. Heat transfer efficiency of ferrofluid with $\phi = 2\%$ as a function of Reynolds number and magnetic strength for (a) solid fin heat sink, (b) porous fin heat sink with $\epsilon = 0.90$.

Fig. 16. Magnetic field influence on the efficiency at different porosity and volume fraction for $\text{Re} = 260$.

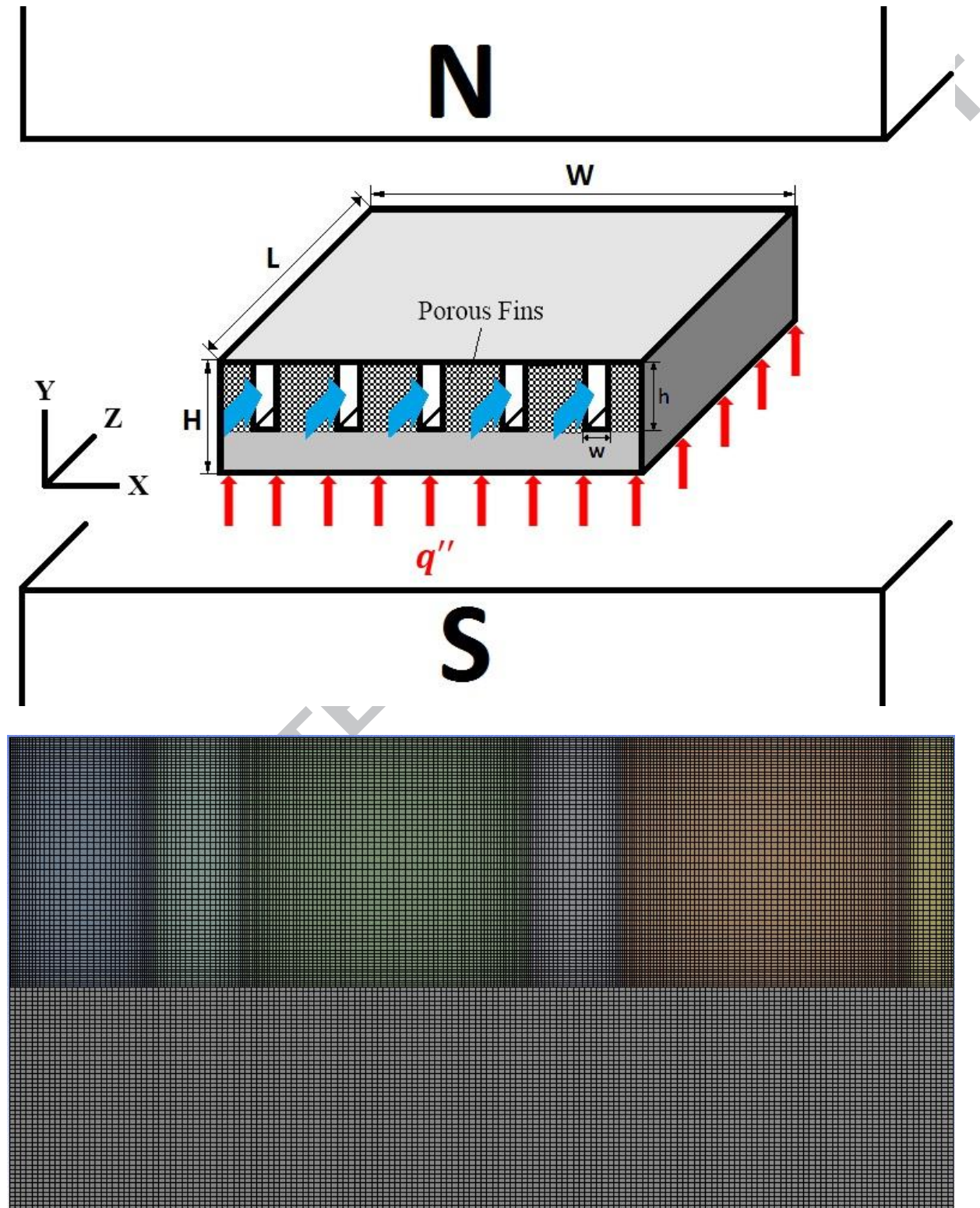
List of tables**Table 1**

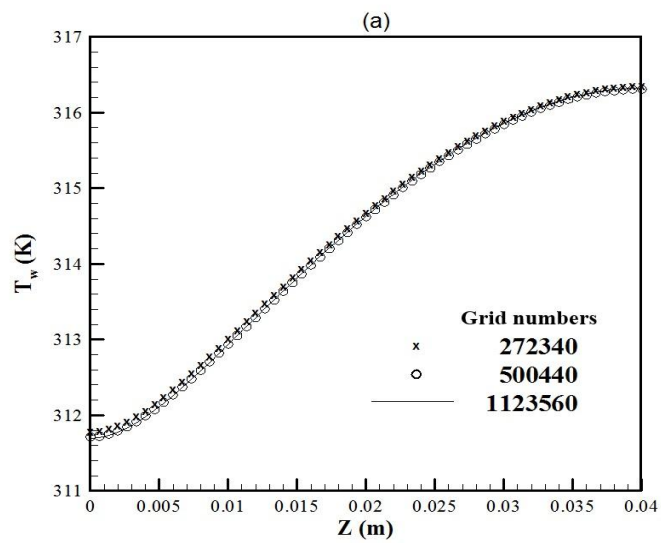
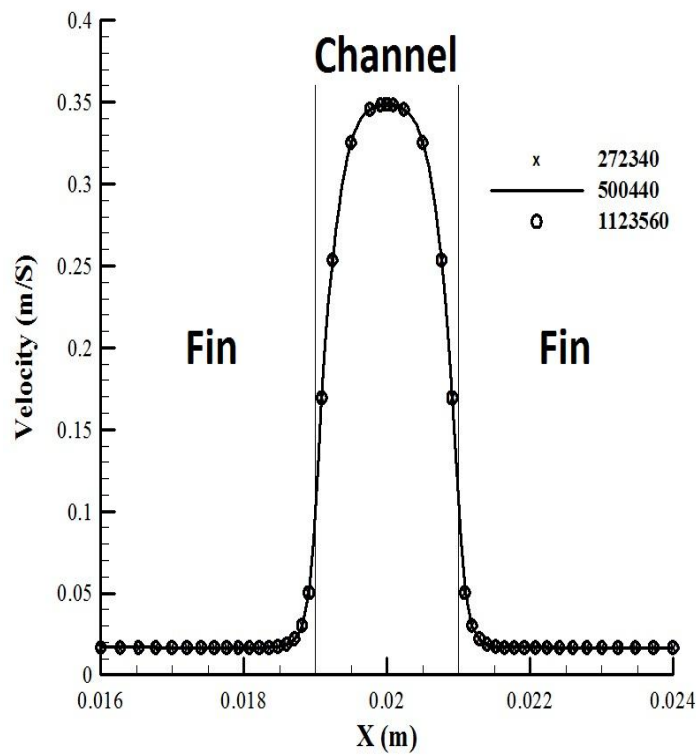
Dimensions of the heat sinks (mm).

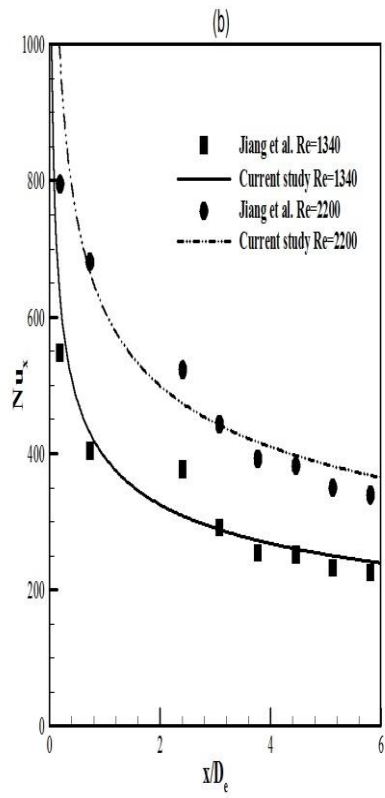
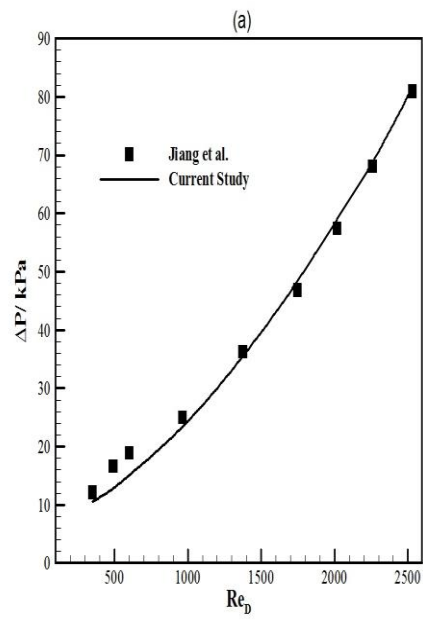
Table 2

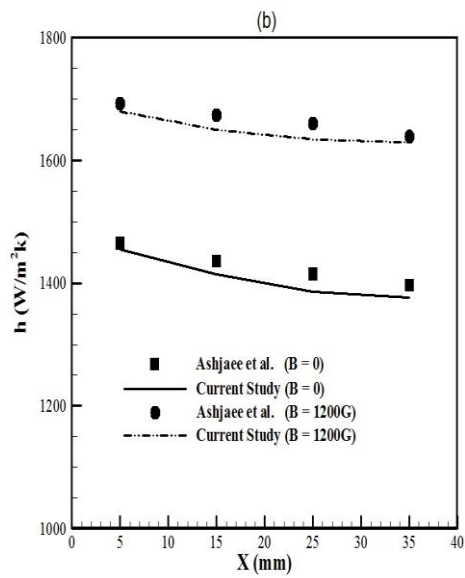
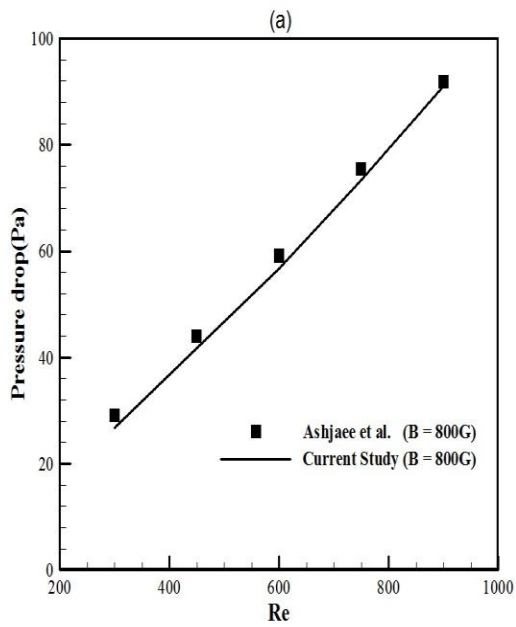
Properties of porous medium and Fe_3O_4 particles.

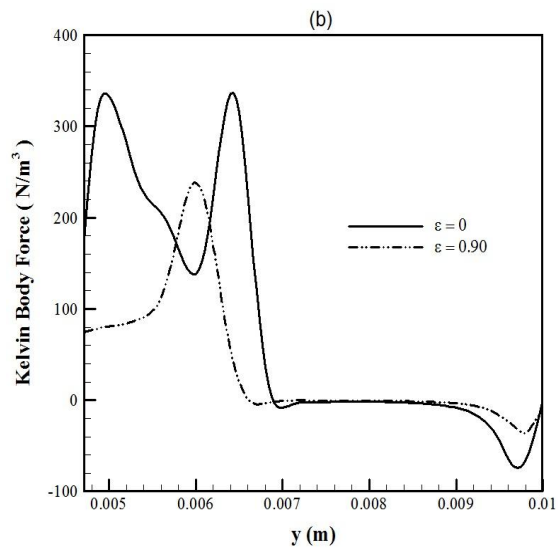
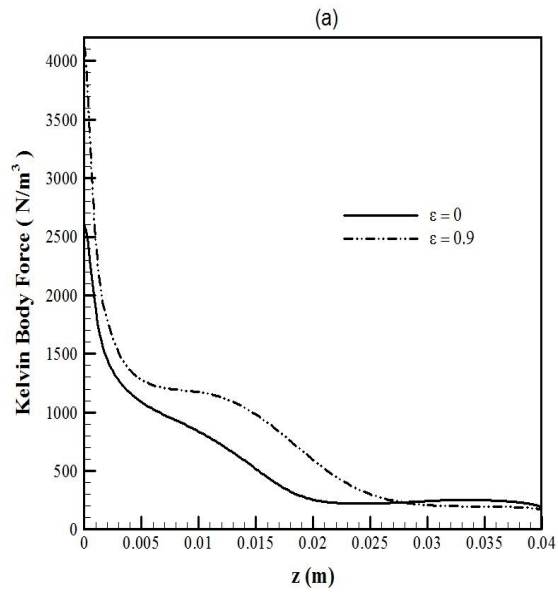
ACCEPTED MANUSCRIPT





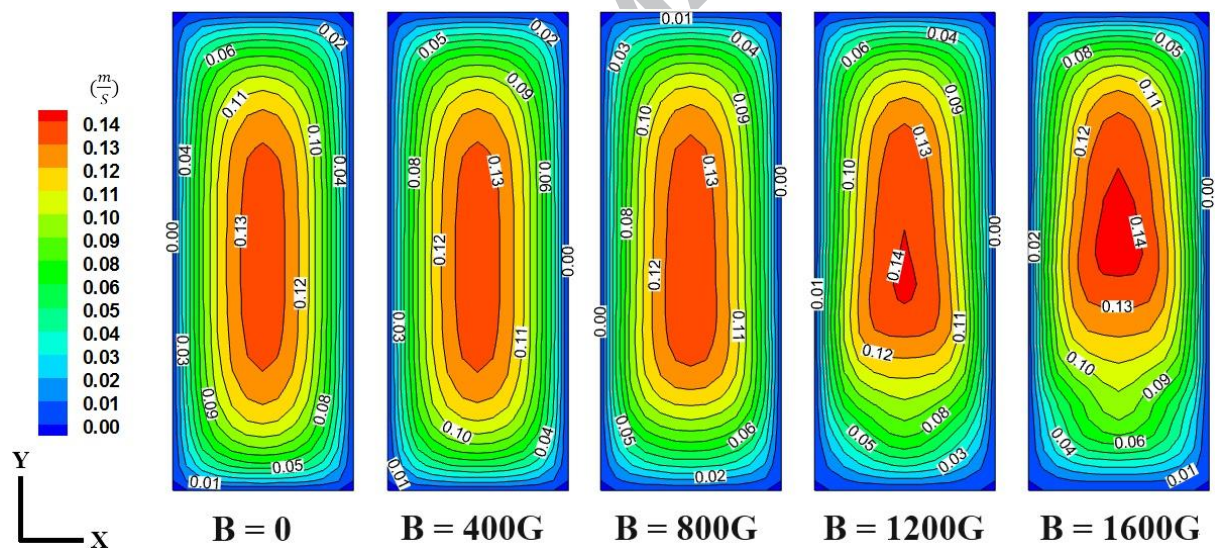
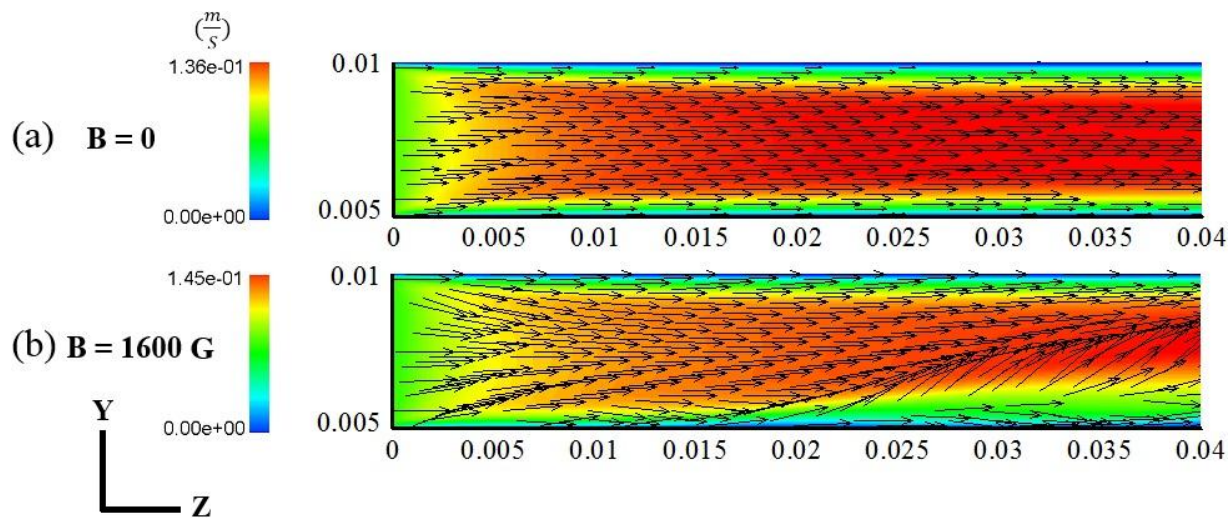


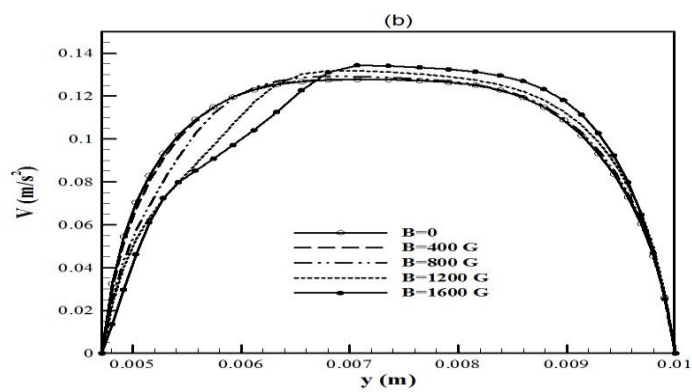
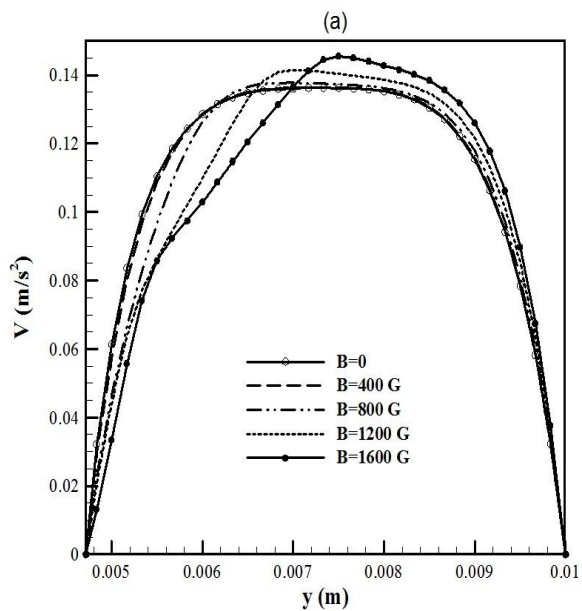


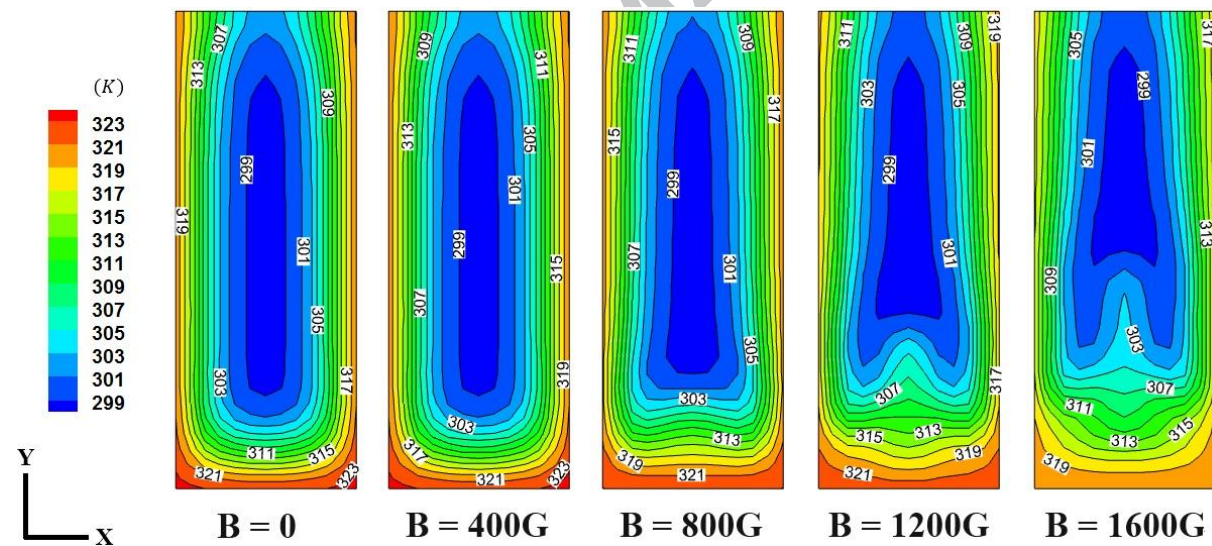
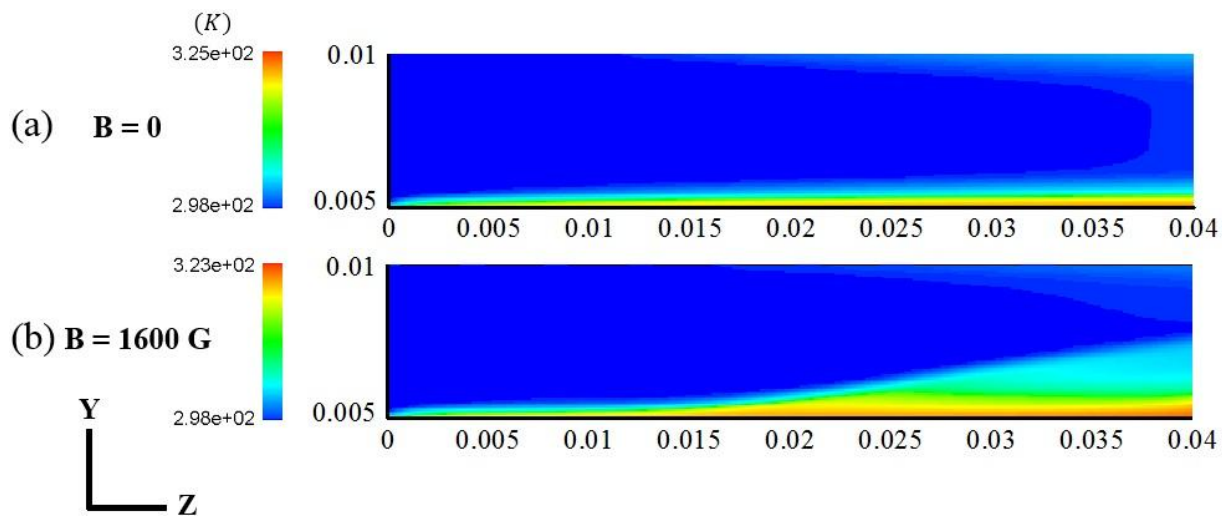


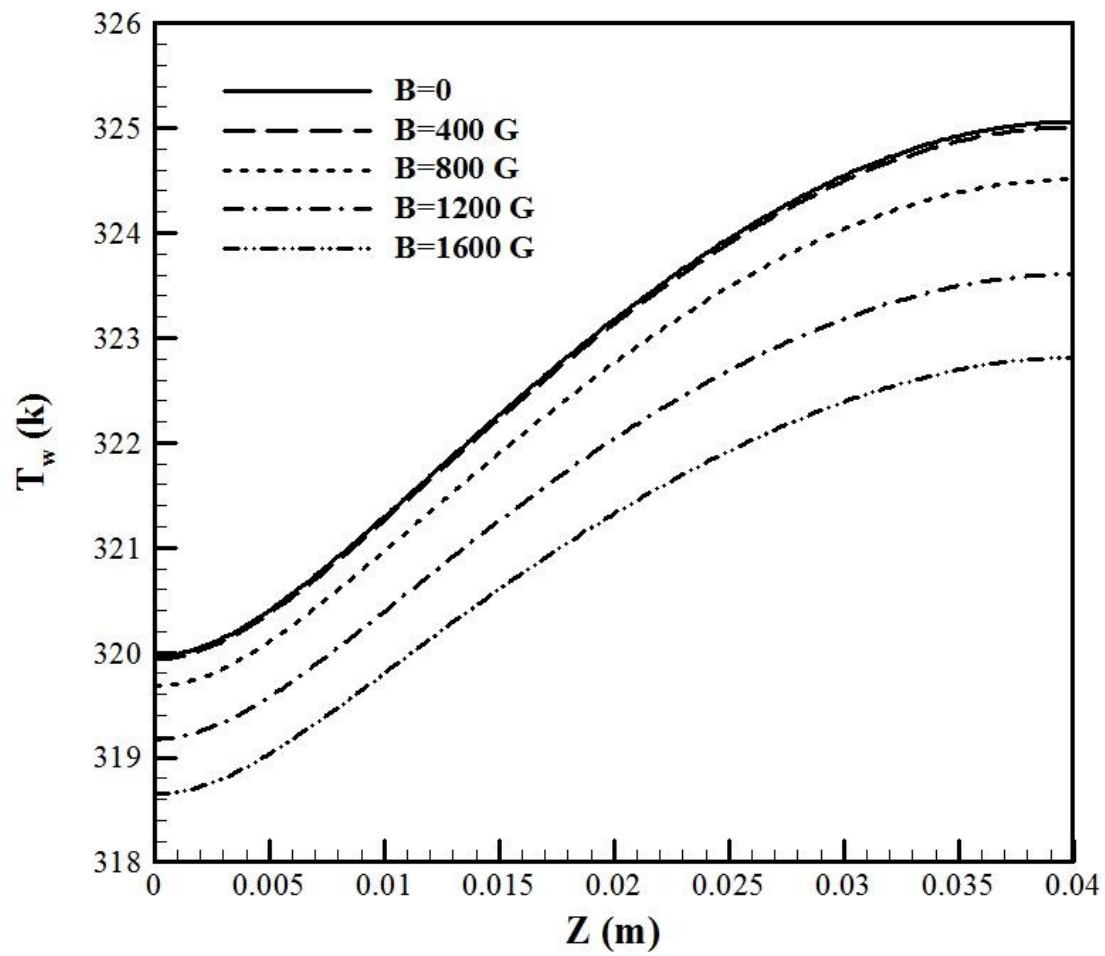
MANUSCRIPT

AC

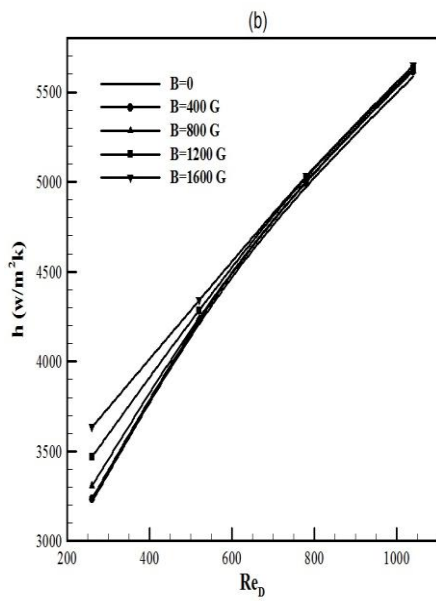
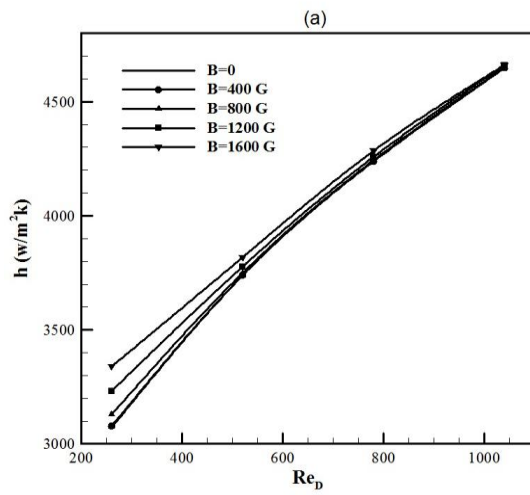


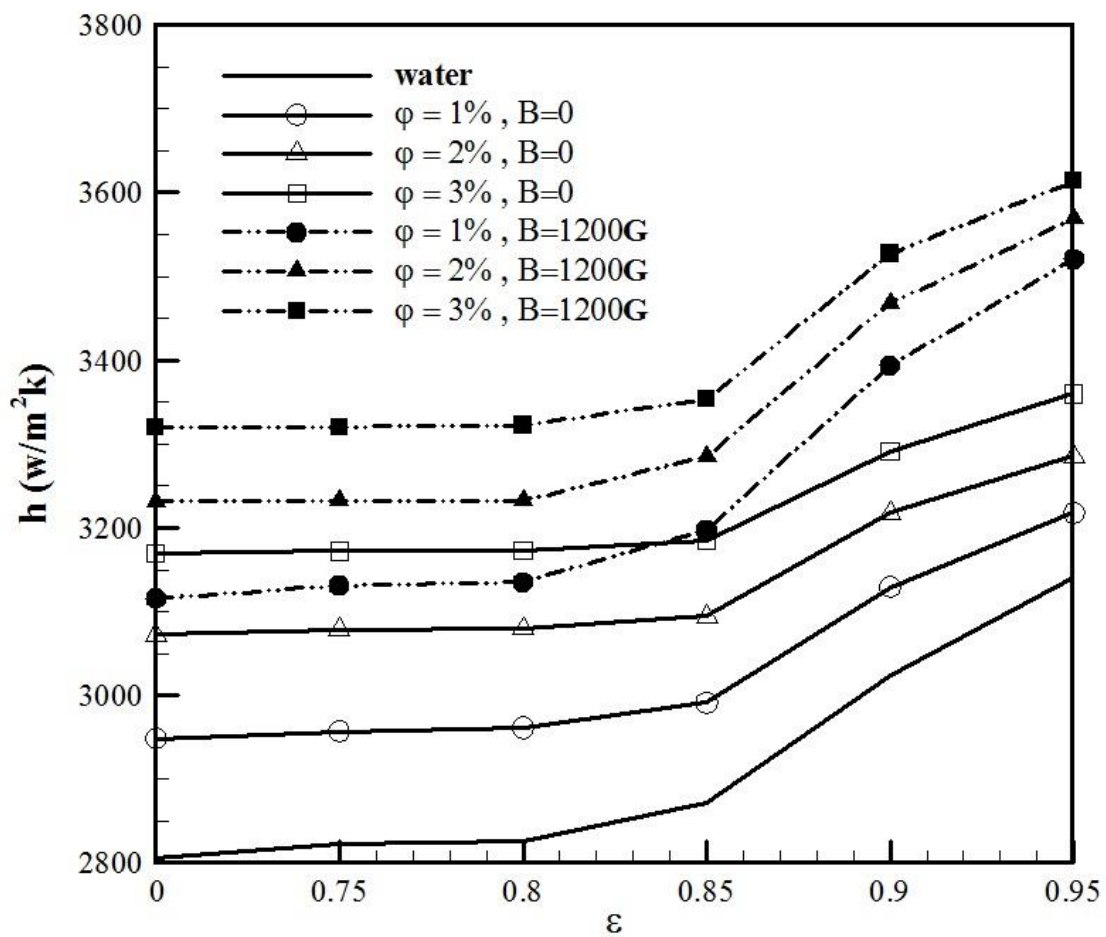




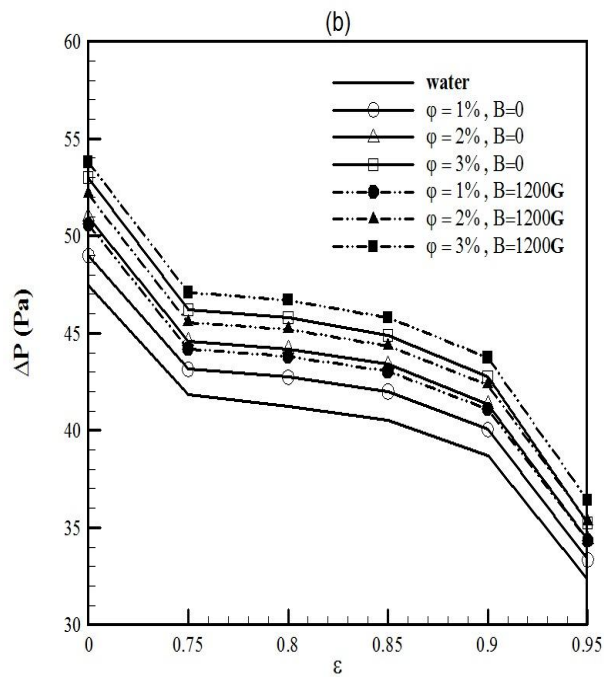
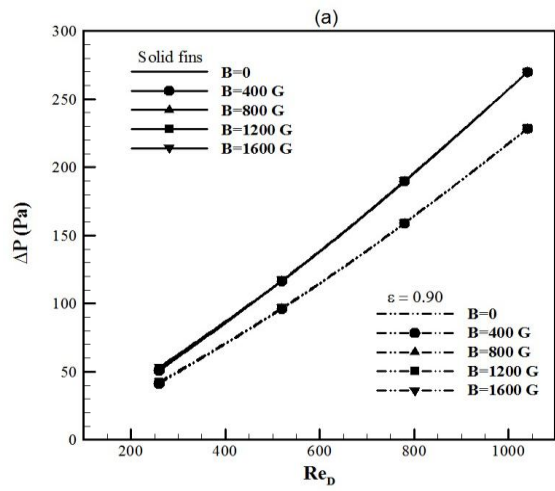


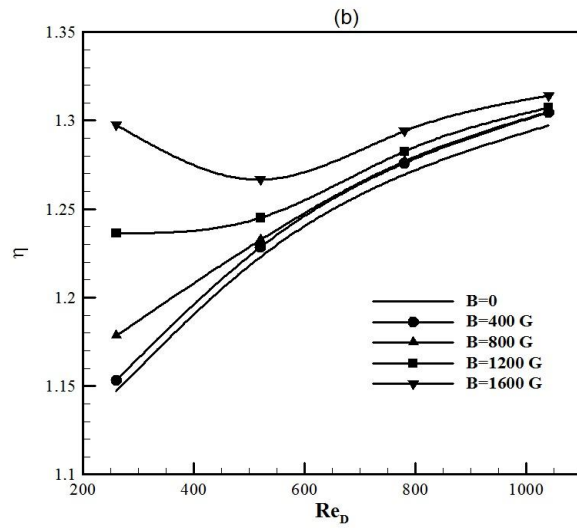
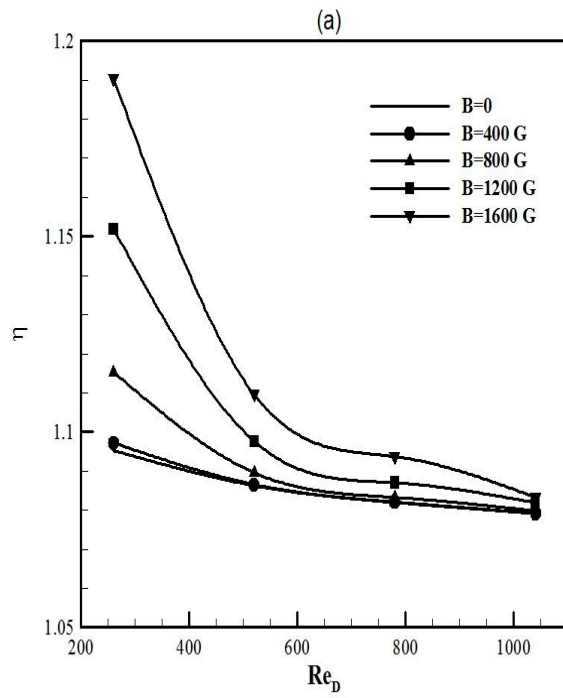
ACCEPT

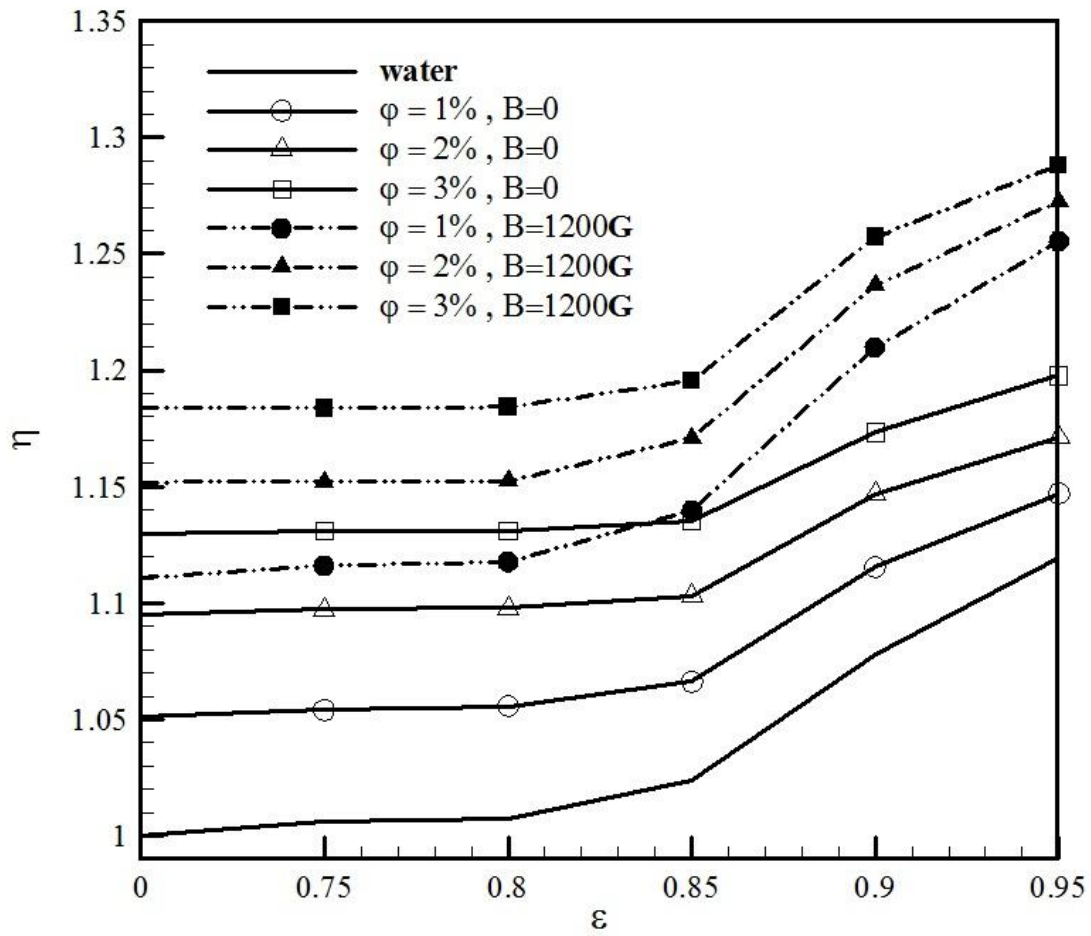




ACCEPT







List of tables

Table 1

Dimensions of the heat sinks (mm).

W	H	L	w	h
40	10	40	2	5.283

Table 2

Properties of porous medium and Fe_3O_4 particles.

Material	Diameter(mm)	k (W/m.K)	C _p (J/kg.K)	ρ (kg/ m ³)
Aluminum	0.1	202.4	871	2719
Fe₃O₄	0.00002	7	640	4950

Highlights

- The magnetic field and porous fins improves heat transfer up to 35%.
- The magnetic field is more effective at low Reynolds numbers.
- The heat transfer changes sharply at high fin porosities.
- Using porous fins decreases the pressure drop compared to the solid fin case.
- The magnetic field has a negligible effect on the pressure drop.